

# X-ray radiation protection aspects during ultrashort laser processing


Cite as: J. Laser Appl. **32**, 022004 (2020); <https://doi.org/10.2351/1.5134778>

Submitted: 01 November 2019 . Accepted: 13 February 2020 . Published Online: 05 March 2020

Herbert Legall , Christoph Schwanke, Jörn Bonse , and Jörg Krüger 

## COLLECTIONS

Note: This paper is part of the Special Collection: Ultrafast Laser Technology 2019.

 This paper was selected as Featured



View Online



Export Citation



CrossMark



Scilight Highlights of the best new research in the physical sciences 

[LEARN MORE!](#)

# X-ray radiation protection aspects during ultrashort laser processing



Cite as: J. Laser Appl. 32, 022004 (2020); doi: 10.2351/1.5134778  
Submitted: 1 November 2019 · Accepted: 13 February 2020 ·  
Published Online: 5 March 2020



Herbert Legall,<sup>a)</sup> Christoph Schwanke, Jörn Bonse, and Jörg Krüger

## AFFILIATIONS

Bundesanstalt für Materialforschung und–prüfung (BAM), Unter den Eichen 87, D-12205 Berlin, Germany

**Note:** This paper is part of the Special Collection: Ultrafast Laser Technology 2019.

<sup>a)</sup>**Author to whom correspondence should be addressed; electronic mail:** [Herbert.Legall@bam.de](mailto:Herbert.Legall@bam.de)

## ABSTRACT

Ultrashort pulse laser processing of materials allows for precise machining with high accuracy. By increasing the repetition rate to several 100 kHz, laser machining becomes quick and cost-effective. Ultrafast laser processing at high repetition rates and peak intensities above  $10^{13}$  W/cm<sup>2</sup> can cause a potential hazard by generation of unwanted x-ray radiation. Therefore, radiation protection must be considered. For 925 fs pulse duration at a center wavelength of 1030 nm, the x-ray emission in air at a repetition rate of 400 kHz was investigated up to a peak intensity of  $2.6 \times 10^{14}$  W/cm<sup>2</sup>. Based on the presented measurements, the properties of potential shielding materials will be discussed. By extending our previous works, a scaling of the x-ray radiation emission to higher peak intensities up to  $10^{15}$  W/cm<sup>2</sup> is described, and emitted x-ray doses are predicted.

**Key words:** laser ablation, ultrashort pulse laser processing, laser-induced x-ray emission, radiation protection

© 2020 Author(s). All article content, except where otherwise noted, is licensed under a Creative Commons Attribution (CC BY) license (<http://creativecommons.org/licenses/by/4.0/>). <https://doi.org/10.2351/1.5134778>

## I. INTRODUCTION

Ultrashort pulse laser processing of solids allows for precise machining with high accuracy because of a weak thermal interaction between the laser beam and the bulk material. Increasing the repetition rate to several 100 kHz made the laser processing of materials attractive for industrial manufacturing processes. Recently, it was shown that ultrafast laser processing can be accompanied by safety relevant emission of x-ray radiation at such high repetition rates if the peak intensity exceeds  $10^{13}$  W/cm<sup>2</sup>.<sup>1</sup> Therefore, x-ray radiation protection in ultrashort laser material processing became a focus of scientific interest.<sup>2–5</sup>

The process of the generation of x-ray radiation builds on the generation of a dense electron plasma produced by the incident laser field. The incident laser field causes free electrons in the solid to oscillate, which subsequently collide with the atoms of the solid, knock electrons out of their shells, which in turn are excited to oscillate in the laser field, until finally a hot mixture of free electrons and ions is present and a laser-induced plasma is born. This laser plasma is usually created by the leading edge of the incoming laser pulse. Subsequently, the high intensity part of the laser pulse

can further heat the plasma. Different mechanisms can contribute to an increase in the average kinetic energy of the electrons (quantified as electron temperature), which finally lead to the emission of x-ray radiation. Thereby, the specific mechanism of laser–plasma interaction influences in a characteristic way both the energetic distribution of the emitted radiation field and the yield with which x-ray photons are generated. A known mechanism leading to x-ray generation in the keV range is the so-called “resonance absorption.”<sup>6</sup> By this collision-less absorption mechanism, plasma electron waves are resonantly excited. The efficiency of this process strongly depends on the polarization state of the laser beam, the pulse duration, and the angle of incidence of the laser pulse. This mechanism was investigated so far mainly in vacuum at low repetition rates in the range up to 1 kHz for  $I\lambda^2 > 10^{15}$  (W/cm<sup>2</sup>) μm<sup>2</sup>, with  $I$  as the peak laser intensity and  $\lambda$  as the laser (center) wavelength. It could be shown that the “resonance absorption” leads to a Maxwellian tail of hot electrons, and the electron temperature scales with  $(I\lambda^2)^{1/3}$ .<sup>6–10</sup> However, these results cannot be simply transferred to the conditions in laser material processing with higher repetition rates at lower peak intensities, since both topographical

changes during laser processing and a heat accumulation in the sample may significantly influence the x-ray generation<sup>4</sup>—the latter by reducing the laser pulse energy consumed in the initial plasma formation stage. To our knowledge, for laser processing in air and in the peak intensity range between  $10^{13}$  W/cm<sup>2</sup> and  $10^{15}$  W/cm<sup>2</sup>, up to now no evidence for this mechanism of x-ray generation was published. However, the scalability of this process may allow to predict a suitable shielding for radiation protection over a broad range of laser peak intensities within certain limits.

In this work, new results on dose measurements of copper and zirconium for intensities up to  $2.6 \times 10^{14}$  W/cm<sup>2</sup> are presented and put into context to other metallic and dielectric materials. A scaling of the x-ray radiation emission for intensities up to  $10^{15}$  W/cm<sup>2</sup> is outlined for aluminum. These results may contribute to radiation protection considerations.

## II. EXPERIMENT

### A. Laser processing

The experiments were performed using a TRUMPF laser system (TruMicro 5050 femto edition) with a laser wavelength of 1030 nm, a maximum pulse repetition rate of 400 kHz, and a pulse duration of 925 fs. Using a galvanometer scanner head (hurrySCAN II 14, SCANLAB GmbH), scan fields with an area of  $10 \times 10$  mm<sup>2</sup> were filled by parallel line scans with an interline distance of 20  $\mu$ m. The line scans were written in a direction away from the x-ray detector positions, with the linear polarization of the laser beam being parallel to the lines. In this arrangement, the highest dose values were obtained.<sup>1,4</sup> The laser beam was focused in air by means of an F-Theta lens with a focal length of 56 mm. The angle of incidence of the laser beam onto the sample plane was  $\sim 0^\circ$ ; the focal beam diameter ( $1/e^2$ ) was  $2w_0 = 10 \pm 1$   $\mu$ m, delivering a maximum peak intensity of  $2.6 \times 10^{14}$  W/cm<sup>2</sup>. For x-ray dose measurements, the samples were irradiated over 5 s with a scan speed of 1000 mm/s. From the accumulated x-ray radiation dose, the dose rate was calculated.

### B. X-ray detection

An active ionization chamber dosimeter (OD-02, STEP GmbH) was used in the accumulation mode for the measurements of the directional dose equivalent  $H'(0.07)$ . The directional dose equivalent  $H'(0.07)$  is related to the skin dose  $H_p(0.07)$ . The deep dose equivalent  $H_p(10)$  is used for monitoring the effective dose of an individual and was evaluated from spectral x-ray measurements. Up to a single pulse x-ray dose of the directional dose equivalent  $H'(0.07) = 0.1$  nSv, the accuracy of the OD-02 could be ensured.<sup>1</sup>

Spectral x-ray measurements were performed using a CdTe spectrometer (X-123CdTe Spectrometer,  $3 \times 3 \times 1$  mm<sup>3</sup>, 100  $\mu$ m Be window, Amptek Inc.). This spectrometer provides a detection efficiency of nearly 100% over a broad range of photon energies up to 50 keV. In comparison, Si detectors lose completely their detection efficiency at photon energies above 20 keV. Even though the CdTe detector is ideally suited for the measurements, it is vulnerable to pile-up. This effect arises if multiple x-ray photons hit the single photon detector during its processing time and are registered as one single photon with higher energy. To minimize the pile-up, the CdTe spectrometer was operated at a large distance of 645 mm to

the laser-generated plasma, and the radiation was additionally attenuated by aluminum filter foils placed in front of the x-ray detector.

## III. X-RAY EMISSION DURING LASER MATERIAL PROCESSING

### A. X-ray dose

In Fig. 1, the maximum x-ray dose rates of the directional dose equivalent  $H'(0.07)$  obtained in air at a distance of 420 mm to the laser irradiation spot are displayed as a function of the peak intensity for different processed materials at a pulse repetition rate of 400 kHz. The laser peak intensity was varied in the experiment by tuning the pulse energy. The maximum x-ray dose was selected from a set of successively performed measurements with constant scan parameters at a fixed position on the sample. For the aluminum-alloy (AlMgSi0.5) and the Gorilla glass, the maximum dose rate was observed already during the first scan. In addition to the data presented in Ref. 1, results for zirconium and copper are shown allowing for a categorization of the materials with respect to the atomic number  $Z$ .

The following conclusions can be drawn from the measured x-ray doses in Fig. 1. First, the x-ray dose increases with the laser peak intensity. Second, in the measured intensity range, a nearly linear increase of the x-ray dose with peak intensity can be observed in the double-logarithmic presentation if no characteristic line emission (K-, L-, and M-shell emission lines) must be considered. The latter is the case for aluminum-alloy and Gorilla glass in the energy range above 2 keV. This is further supported by the fact that the maximum deviation is found at different peak intensities for different materials, which might be explained by the characteristic absorption edges located at different photon energies. Finally, the results in Fig. 1 show that, even if the x-ray dose tends to rise

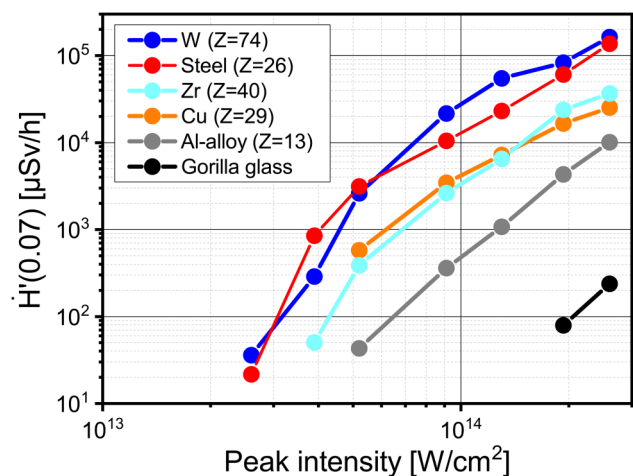


FIG. 1. Measured dose rates  $H'(0.07)$  in dependence on the material and the incident laser peak intensity. Different target materials were investigated [tungsten, steel (S235JR), aluminum-alloy (AlMgSi0.5), zirconium, copper, and Gorilla glass] using the ionization chamber dosimeter OD-02 at a distance of 420 mm in air. The peak intensity was varied between  $2.6 \times 10^{13}$  and  $2.6 \times 10^{14}$  W/cm<sup>2</sup>.

with the atomic number  $Z$ , elements with higher atomic number not always deliver higher x-ray doses, compare, e.g., the curves for steel (S235JR) and zirconium. The latter finding is in contradiction to established scaling laws found for ultrashort pulse laser material interaction at low pulse repetition rates<sup>9,10</sup> and can only be understood by considering further material properties (e.g., thermal parameters), which might become relevant at high laser pulse repetition rates. For a scaling of the x-ray dose with the peak intensity, the characteristic line emission and a pre-structuring of the sample surface must be considered. Moreover, the dependence of the generated x-ray dose on the atomic number must be related to the specific laser and processing parameters applied.

### B. Spectral x-ray dose

As the attenuation of a shielding material depends on the spectral distribution of the incident x-ray radiation, a shielding factor can only be calculated if the spectral photon flux is exactly known. For this reason, spectral x-ray measurements were performed. The evaluation of the spectral dose rates from measured x-ray spectra was already demonstrated in Ref. 1. It was shown that from the x-ray spectrum the spectral photon flux and from the spectral photon flux the spectral dose rate can be calculated by using energy dependent photon-to-dose conversion factors.<sup>11</sup> Integration over the distribution of the spectral dose rates finally delivers the effective dose rate.

In Fig. 2, two tungsten x-ray spectra are shown, which were constructed based on spectral measurements with different filter thicknesses (a 45  $\mu\text{m}$  thick aluminum filter at  $5.2 \times 10^{13} \text{ W/cm}^2$ , and 45 and 362  $\mu\text{m}$  thick aluminum filters at  $2.6 \times 10^{14} \text{ W/cm}^2$ ) in front of the CdTe detector according to the procedure presented in Ref. 1. The x-ray spectra displayed in Fig. 2 were measured in air at a laser repetition rate of 400 kHz with tungsten as a sample material at a peak intensity of  $5.2 \times 10^{13}$  and  $2.6 \times 10^{14} \text{ W/cm}^2$ , and corrected for

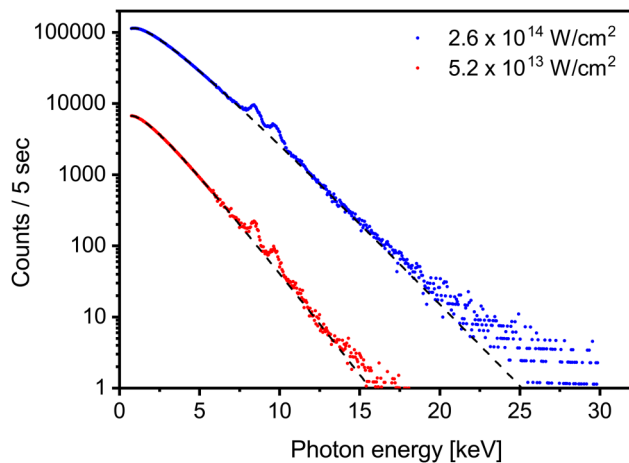


**FIG. 2.** X-ray spectra in vacuum constructed from measured emission spectra after correction for air absorption. The measurements were performed in air with tungsten as the target material at intensities of  $5.2 \times 10^{13}$  and  $2.6 \times 10^{14} \text{ W/cm}^2$  at a distance of 645 mm. The spectra were extrapolated to lower x-ray photon energies by a Maxwellian distribution (black dashed lines).

air absorption. The dashed curves in Fig. 2 represent the Maxwell Boltzmann distributions with which the Bremsstrahlung spectrum was approximated, according to the following formula:<sup>6</sup>

$$f_{\text{Maxwell}}(E)dE = \sqrt{\frac{4E}{\pi(k_B T_e)^3}} \cdot \exp\left(-\frac{E}{k_B T_e}\right) dE, \quad (1)$$

with  $k_B = 8.6 \times 10^{-5} \text{ eV/K}$  and  $1 \text{ eV} \triangleq 1.2 \times 10^4 \text{ K}$ ,  $E$  is the x-ray photon energy,  $k_B$  denotes the Boltzmann constant, and  $T_e$  is the electron temperature (expressed in keV).

The spectral personal dose rates  $\dot{H}_p(0.07)$  and  $\dot{H}_p(10)$  for tungsten at the peak intensity of  $5.2 \times 10^{13} \text{ W/cm}^2$  are shown in Fig. 3 for two different distances to the ablation source. Integration over the spectral dose rates  $\dot{H}_p(0.07)$  in Fig. 3(a) yields an overall dose rate of  $\dot{H}_p(0.07) = 4 \text{ mSv/h}$  in air at a distance of 420 mm, which corresponds well to the dose rate of 2.61 mSv/h (cp. Fig. 1) simultaneously

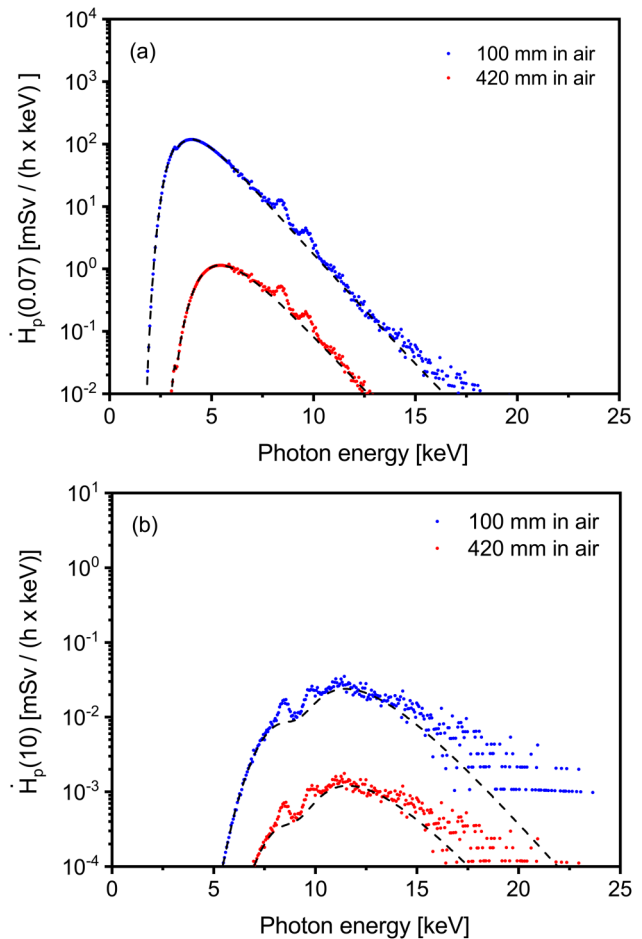


**FIG. 3.** Spectral dose rates  $\dot{H}_p(0.07)$  (a) and  $\dot{H}_p(10)$  (b) for tungsten irradiated at a peak intensity of  $5.2 \times 10^{13} \text{ W/cm}^2$  for two distances (100 and 420 mm) calculated in air from the spectrum in Fig. 2. Additionally, the spectral dose rates calculated from the Maxwellian distribution are shown (black dashed lines).

**TABLE I.** Minimum thicknesses required for x-ray shielding by iron and aluminum for tungsten samples processed at a pulse duration of 925 fs, a laser repetition rate of 400 kHz at a wavelength of 1030 nm, and the peak intensities as noted.

Distance to the irradiation spot (mm)	Iron, $2.6 \times 10^{14}$ W/cm <sup>2</sup> (mm)	Aluminum, $2.6 \times 10^{14}$ W/cm <sup>2</sup> (mm)	Iron, $5.2 \times 10^{13}$ W/cm <sup>2</sup> (mm)	Aluminum, $5.2 \times 10^{13}$ W/cm <sup>2</sup> (mm)
100	0.537	12.311	0.125	2.824
200	0.386	8.879	0.074	1.639
300	0.309	7.100	0.051	1.100
420	0.252	5.777	0.034	0.731
500	0.225	5.151	0.027	0.564

measured with the OD-02 dosimeter, when taking into account the lower sensitivity of OD-02 at photon energies below 6 keV in comparison to the CdTe detector. For the overall dose rate  $\dot{H}_p(10)$  in air at a distance of 420 mm, a value of 0.08 mSv/h was evaluated from Fig. 3(b). For comparison, the overall dose rates of  $\dot{H}_p(0.07) = 156$  mSv/h and  $\dot{H}_p(10) = 0.68$  mSv/h for the peak intensity of  $2.6 \times 10^{14}$  W/cm<sup>2</sup> in air were already presented in Ref. 1.

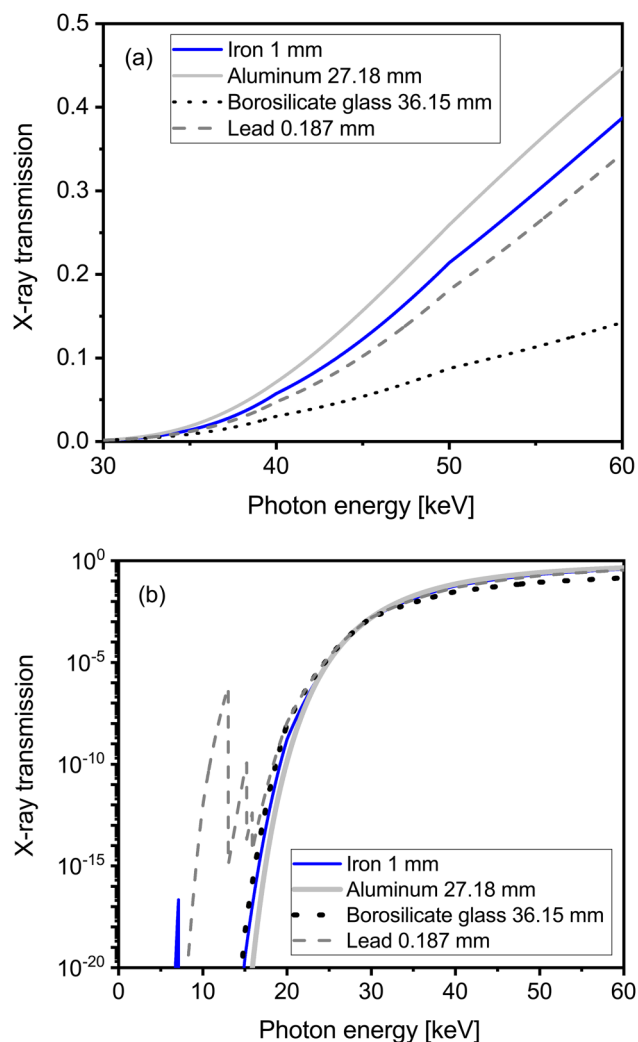
#### IV. RADIATION PROTECTION

##### A. Shielding considerations

To estimate an adequate protection shielding from the x-ray spectra presented in Fig. 2, the effective dose rates were calculated behind two different shielding materials (iron and aluminum). In Table I, various thicknesses of these shielding materials are presented ensuring that the regulatory radiation limit for the effective dose rate of  $\dot{H}_p(10) = 1$   $\mu$ Sv/h will not be exceeded. The calculations were performed for different distances to the laser irradiation spot. The values in Table I show that aluminum is only restrictedly suitable for the shielding of a material processing facility. Note that the calculated shielding thicknesses in Table I are minimum values. In practice, these thicknesses should be chosen significantly larger (e.g., twice the thicknesses given in Table I) in order to completely exclude an x-ray exposition of individuals working at these facilities.

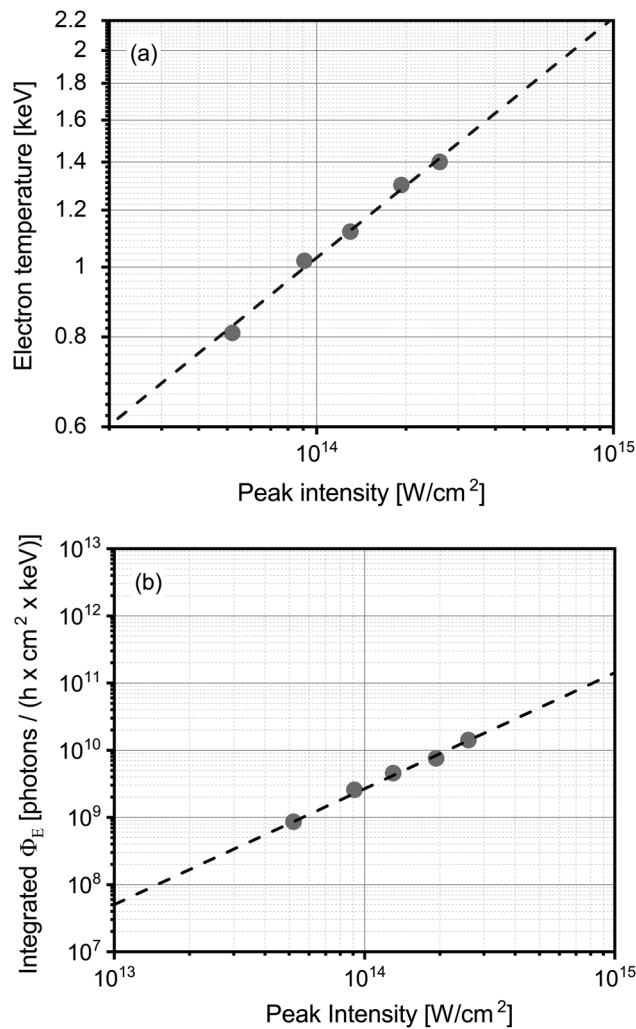
##### B. Shielding materials

For the laser setup with a maximum peak intensity of  $2.6 \times 10^{14}$  W/cm<sup>2</sup>, the dose relevant x-ray emission in the investigated intensity range is limited to photon energies below 30 keV.<sup>1</sup> For peak intensities above  $2.6 \times 10^{14}$  W/cm<sup>2</sup>, significant contributions to the dose above 30 keV can be expected. Consequently, it can be useful to compare the shielding efficiency of different materials at photon energies above 30 keV. In Fig. 4, the transmission of four different materials is shown as a function of the x-ray photon energy up to 60 keV. The transmission curves were calculated by using mass attenuation coefficients provided by the National Institute of Standards and Technology (NIST), USA.<sup>12</sup> The thickness of the materials was adjusted such that the attenuation was equal for all materials at a photon energy of 30 keV. It can be seen that the attenuation of the x-ray radiation strongly decreases for photon energies above 30 keV. An equivalent shielding thickness of different materials for attenuation up to 60 keV can be conservatively

**FIG. 4.** X-ray transmission of different shielding materials according to mass attenuation coefficients provided by the NIST. The thickness of the materials was chosen in a way that the attenuation at the photon energy of 30 keV was equal for all materials. (a) Linear ordinate; (b) logarithmic ordinate.

**TABLE II.** Equivalent thickness of different shielding materials for x-ray protection up to photon energies of 60 keV in relation to iron.

Material	Equivalent thickness (mm)
Iron	1
Aluminum	32
Borosilicate glass	40
Lead	0.5

**FIG. 5.** Electron temperature (a) and integrated photon flux calculated at a distance of 420 mm in vacuum (b) evaluated for the aluminum-alloy from spectral measurements at different peak intensities at a pulse duration of 925 fs, a laser wavelength of 1030 nm, and a repetition rate of 400 kHz. The fits indicate a scaling of the electron temperature with peak intensity of  $I^{1/3}$  and a scaling of the integrated photon flux with peak intensity of  $I^{1.7}$ . The data points are based on measurements; the dashed lines are the corresponding power laws.

estimated as shown in Table II. It is obvious from these data that for x-ray photon energies up to 60 keV, aluminum and borosilicate glass require a 30–40 times larger thickness to obtain the same protection level as iron (or steel).

### C. Scaling of the x-ray emission to higher peak intensities

Finally, it will be discussed whether a scaling of the x-ray emission to higher peak intensities is possible. In Fig. 5, the electron temperature (a) and the integrated photon flux in vacuum at a distance of 420 mm to the ablation spot (b) are displayed for the laser-irradiated aluminum-alloy. These quantities were calculated from the x-ray spectra measured simultaneously to the dose measurements (Fig. 1). Both quantities scale linearly in the double-logarithmic presentation, i.e., with power laws. While the electron temperature scales with the peak intensity as  $I^{1/3}$ , the integrated photon flux  $\Phi_E$  scales with  $I^{1.7}$ . The scaling of electron temperature with  $I^{1/3}$  suggests that the “resonance absorption”<sup>6–10</sup> is the dominant mechanism of x-ray generation here.

By scaling the amplitude of the Maxwellian distribution in Eq. (1), the x-ray spectrum can be calculated for a selected electron temperature [dashed line in Fig. 5(a)] along with the associated integrated photon flux [dashed line in Fig. 5(b)]. This was exemplarily done for a peak intensity of 10<sup>15</sup> W/cm<sup>2</sup>. For an aluminum-alloy at an electron temperature of 2.2 keV [Fig. 5(a)] at a peak intensity of 10<sup>15</sup> W/cm<sup>2</sup>, a dose rate of  $\dot{H}_p(0.07) = 320$  mSv/h can be deduced from the scaled spectrum for a distance of 420 mm to the ablation spot in air. For other materials, the scaling becomes more intricate, due to the additional contribution from the characteristic emission lines to the total x-ray dose rate.

### V. CONCLUSIONS

Ultrashort pulse laser material processing was performed employing 925-fs pulses at a center wavelength of 1030 nm, a repetition rate of 400 kHz, and a maximum peak intensity of  $2.6 \times 10^{14}$  W/cm<sup>2</sup>. The dependence of the x-ray dose on the atomic number of the sample materials was studied revealing that the x-ray dose does not monotonously scale with the atomic number. Additional material properties must be considered for high laser pulse repetition rates. For the aluminum-alloy, a nearly linear increase of the x-ray dose with peak intensity was observed in a double-logarithmic representation for peak intensities between  $5.2 \times 10^{13}$  and  $2.6 \times 10^{14}$  W/cm<sup>2</sup>. From the spectral measurements, the scaling of the electron temperature with the peak intensity was deduced, which is in line with the “resonance absorption” mechanism reported earlier for regimes with higher intensities. Here, the electron temperature scales with the peak intensity as  $I^{1/3}$  and the integrated photon flux in the Bremsstrahlung continuum with  $I^{1.7}$  for aluminum-alloy. For other metals, the characteristic x-ray radiation influences the dose measurements leading to a deviation from the power laws. Using the scaling laws, a spectral dose can be calculated. Exemplarily, a dose rate of  $\dot{H}_p(0.07) = 320$  mSv/h for a peak intensity of 10<sup>15</sup> W/cm<sup>2</sup> was deduced for the aluminum-alloy. For x-ray photon energies exceeding 30 keV, shielding made of aluminum and borosilicate glass requires a 30–40 times larger thickness to obtain the same protection level as iron or steel.

## ACKNOWLEDGMENTS

The authors gratefully acknowledge financial support from the German Federal Ministry of Education and Research (BMBF) in the funding program Photonics Research Germany under Contract No. 13N14249.

## REFERENCES

- <sup>1</sup>H. Legall, C. Schwanke, S. Pentzien, G. Dittmar, J. Bonse, and J. Krüger, "X-ray emission as a potential hazard during ultra-short pulse laser material processing," *Appl. Phys. A* **124**, 407 (2018).
- <sup>2</sup>R. Behrens, B. Pullner, and M. Reginatto, "X-ray emission from material processing lasers," *Radiat. Prot. Dosim.* **126**, 1–14 (2018).
- <sup>3</sup>H. Legall, C. Schwanke, J. Bonse, and J. Krüger, "X-ray emission during ultra-short pulse laser processing," *Proc. SPIE* **10908**, 1090802 (2019).
- <sup>4</sup>H. Legall, C. Schwanke, J. Bonse, and J. Krüger, "The influence of processing parameters on x-ray emission during ultra-short pulse laser machining," *Appl. Phys. A* **125**, 570 (2019).
- <sup>5</sup>R. Weber, R. Giedl-Wagner, D. J. Förster, A. Pauli, T. Graf, and J. Balmer, "Expected x-ray dose rates resulting from industrial ultrafast laser applications," *Appl. Phys. A* **125**, 635 (2019).
- <sup>6</sup>W. Krueer, *The Physics of Laser Plasma Interactions* (CRC Press, Boca Raton, 2018).
- <sup>7</sup>D. D. Meyerhofer, H. Chen, J. A. Delettrez, B. Soom, S. Uchida, and B. Yaakobi, "Resonance absorption in high-intensity contrast, picosecond laser-plasma interactions," *Phys. Fluids B* **5**, 2584 (1993).
- <sup>8</sup>P. Gibbon, "Physics of high-intensity laser-plasma interactions," *Riv. Nuovo Cimento Soc. Ital. Fis.* **35**, 607 (2012).
- <sup>9</sup>J. Yu, Z. Jiang, J. C. Kieffer, and A. Krol, "Hard x-ray emission in high intensity femtosecond laser–target interaction," *Phys. Plasmas* **6**, 1318 (1999).
- <sup>10</sup>J. C. Kieffer, A. Krol, Z. Jiang, C. C. Chamberlain, E. Scalzetti, and Z. Ichalalene, "Future of laser-based x-ray sources for medical imaging," *Appl. Phys. B* **74**, S75–S81 (2002).
- <sup>11</sup>K. G. Veinot and N. E. Hertel, "Personal dose equivalent conversion coefficients for photons to 1 GeV," *Radiat. Prot. Dosim.* **145**, 28–35 (2011).
- <sup>12</sup>J. H. Hubbell and S. M. Seltzer, "Tables of x-ray mass attenuation coefficients and mass energy-absorption coefficients from 1 keV to 20 MeV for elements Z = 1 to 92 and 48 additional substances of dosimetric interest," in *X-ray mass attenuation coefficients*, NIST Standard Reference Database 126.